Open Archive Toulouse Archive Ouverte (OATAO)

OATAO is an open access repository that collects the work of Toulouse researchers and makes it freely available over the web where possible.

To link to this article :
URL : http://dx.doi.org/10.1179/174367508X297812

Any correspondence concerning this service should be sent to the repository administrator: staff-oatao@inp-toulouse.fr

Sintering and densification of nanocrystalline ceramic oxide powders: a review

R. Chaim*[1], M. Levin[1], A. Shlayer[1] and C. Estournes[2]

Observation of the unconventional properties and material behaviour expected in the nanometre grain size range necessitates the fabrication of fully dense bulk nanostructured ceramics. This is achieved by the application of ceramic nanoparticles and suitable densification conditions, both for the green and sintered compacts. Various sintering and densification strategies were adopted, including pressureless sintering, hot pressing, hot isostatic pressing, microwave sintering, sinter forging, and spark plasma sintering. The theoretical aspects and characteristics of these processing techniques, in conjunction with densification mechanisms in the nanocrystalline oxides, were discussed. Spherical nanoparticles with narrow size distribution are crucial to obtain homogeneous density and low pore-to-particle-size ratio in the green compacts, and to preserve the nanograin size at full densification. High applied pressure is beneficial via the densification mechanisms of nanoparticle rearrangement and sliding, plastic deformation, and pore shrinkage. Low temperature mass transport by surface diffusion during the spark plasma sintering of nanoparticles can lead to rapid densification kinetics with negligible grain growth.

Keywords: Sintering, Densification, Nanocrystalline, Ceramics, Nanoparticles, Spark plasma sintering, Oxides

Introduction

During the last decade, extensive efforts have been made to develop fabrication techniques and new sintering methodologies for full densification of bulk nanocrystalline ceramics. These efforts were motivated by the theoretical expectations that many properties of the nanocrystalline materials in general, and of nanocrystalline ceramics in particular, will change significantly with the decrease of grain size into the nanometre range. In the light of both scientific and technological importance of these sintering methodologies, comprehensive reviews were published more than a decade ago.[1–5]

At present, the major interest in the densification of nanocrystalline ceramics is not only in preserving the nanocrystalline character of the grains but also in obtaining fully dense ceramics. Unlike the conventional technical ceramics, the pore volume fraction in bulk nanocrystalline ceramics should be limited below a few tens of PPM. These microstructural characteristics are necessary in examining the sole effect of the grain size on the physical, mechanical, and optical properties of ceramics with nanometre grain size. The present paper attempts to examine the effects of the microstructure and process variables at different stages during the sintering and densification of nanocrystalline ceramics.

Various aspects of pore elimination during the densification of ceramic powder compacts were thoroughly investigated.[6–10] These include the morphological and topological characteristics of the pores and the grains, such as shape, size, and size distribution, the interface and surface energies and mobilities of the grain boundaries and the pores, as well as the dominating sintering mechanisms.[10] Based on the interfacial energy considerations, pores with critical coordination number (6 in two dimensions; 12 in three dimensions) may be stable and will not shrink during the sintering. These geometrical constraints impose the critical pore to the grain size ratio above which the pore is stable. Since this pore to the grain size ratio in ceramics typically ranges between 0·5 and 1·5, the pore and the grain size are closely related.[6] Assuming homogeneous and randomly closed packed green compacts, the average pore size is directly related to the average particle size. Consequently, the application of nanocrystalline ceramic particles for homogeneous green compacts is expected to result in nanometric pores with higher mobility, and in turn, to faster densification kinetics. This is the main advantage of the nanocrystalline ceramic powders which are used for the fabrication of dense ceramics.

As will be shown below, the main problems during the densification of the nanoparticle clusters and the preservation of the nanostructure are associated with their coarsening and pore growth at the early stages of sintering, as well as grain growth at the final stage of sintering. As long as the pore mobility is higher than, or comparable to the grain boundary (gb) mobility, the

[1]Department of Materials Engineering, Technion – Israel Institute of Technology, Haifa 32000, Israel
[2]Institut Carnot CIRIMAT, UMR CNRS-UPS-INP 5085, Bat. 2R1, Universite Paul Sabatier 31062 Toulouse Cedex 9, France

*Corresponding author, email rchaim@technion.ac.il
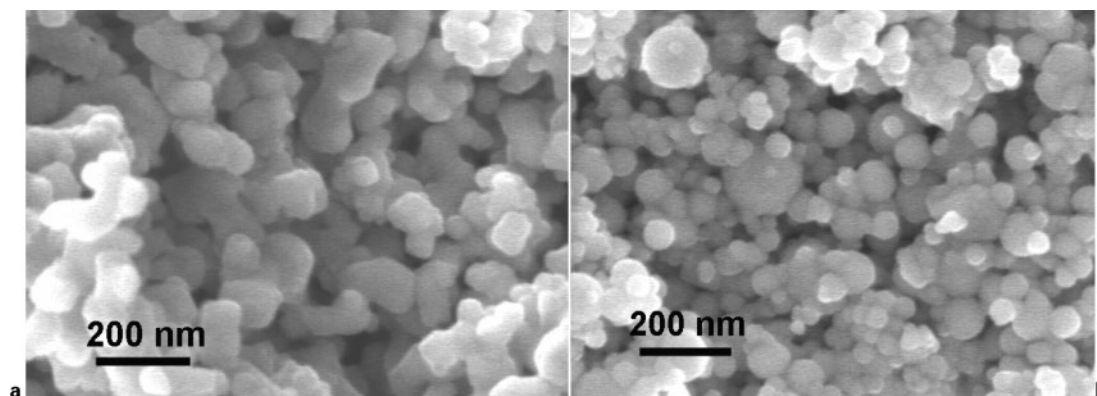
1 HRSEM images of nanocrystalline yttrium aluminium garnet (nc-YAG) powders synthesised by *a* wet chemical precipitation and *b* flame spray pyrolysis: agglomerated nature of equiaxed, polyhedral shape particles in *a* versus agglomerate free spherical shape particles in *b* are visible; both powders exhibited lognormal particle size distribution with mean particle diameter of 74±32 and 34±17 nm respectively

pore is attached to the grain boundary and may be eliminated by vacancy diffusion along the gb's. The effect of the grain size on the pore elimination during densification was studied by Monte Carlo simulations.[11] It was found that once the pore size becomes larger than the grain size, its elimination time is proportional to the fourth order of the pore diameter. This indicates that such pores practically cannot be eliminated. Consequently, for the pore to be eliminated, the grain size should be kept below a critical value.

Nanoparticles and conventional sintering

In recent years, old and novel routes were adopted for the synthesis of nanometric ceramic particles in commercial quantities. These include:

(i) sol-gel and chemical wet methods for precipitation of oxides mainly from salt solutions
(ii) flame and spray pyrolysis of both oxide and non-oxide powders, using inorganic solutions
(iii) chemical vapour techniques for nanopowder synthesis.

These techniques and their modifications often result in specific powder characteristics, such as particle shape and morphology, size, and size distribution that may have crucial impacts on the homogeneity and density of the green compacts.

The chemical wet routes often result in amorphous precursors that by calcination at high temperatures crystallise to the final nanocrystalline powder. The chemical vapour synthesis, on the other hand, results mainly in crystalline nanopowders. These synthesis routes are often characterised by polyhedral shaped nanocrystals that are either partially sintered, or exhibit some degree of agglomeration/aggregation (Fig. 1*a*). However, the as-precipitated particle morphology, its size and distribution may be controlled using appropriate surfactants, calcination temperature, and duration.[12–14] On the other hand, recent spray and flame related techniques can result in non-agglomerated ceramic nanopowders with either polyhedral or spherical morphology (Fig. 1*b*).

The high specific surface of the nanocrystalline powders often accounts for their high reactivity and driving force for sintering. Nevertheless, full densification of nanocrystalline ceramic compacts by pressureless sintering is still challenging. This can simply be explained by the propensity of the nanocrystalline powder to coarsening during the heating stage. The typical heating rates used for the conventional sintering techniques are of the order of 2 to 15 °C/min. Then a few hours were spent for heating the green compact to the sintering temperatures (i.e. 800 to 1500°C), that suffices for significant particle coarsening by surface diffusion. This effect often leads to heterogeneous shrinkage if agglomerated powders are used. Therefore, many pressureless sintering studies with different strategies have only resulted in partial densification of various nanocrystalline oxide powders.[15–27]

As was discussed by many investigators, the two processes of densification by pore closure and grain growth are competitive and depend on temperature and grain size. Assuming that surface and grain boundary diffusions dominate in nanocrystalline compacts, the corresponding rates of densification and grain growth during the intermediate and final stages of pressureless sintering may be expressed respectively as[28]

$$\frac{1}{\rho}\frac{\mathrm{d}\rho}{\mathrm{d}t} = \frac{733 D_{gb}\delta_{gb}\gamma_{SV}V_m}{RTG^4\rho} \tag{1}$$

and

$$\frac{1}{G}\frac{\mathrm{d}G}{\mathrm{d}t} = \frac{110 D_S\delta_S\gamma_{gb}V_m}{RTG^4}(1-\rho)^{-\frac{4}{3}} \tag{2}$$

where D_{gb} and D_S are the diffusivities at the grain boundary and surface, δ_{gb} and δ_S are the grain boundary and surface thicknesses, where effective diffusion takes place, γ_{SV} and γ_{gb} are the specific surface and grain boundary energies, G is the grain size, ρ is the density, V_m is the molar volume, T is the absolute temperature, and R is the gas constant.

Following equations (1) and (2) as was discussed by Rahaman[29] and Kang,[30] it can be shown that under the present assumptions the ratio of the two process rates is independent of grain size. Consequently, low sintering temperatures are preferred to keep this ratio low and thus preserve the nanostructure character during densification. Furthermore, where lattice diffusion dominates at higher sintering temperatures, the ratio of the processes is grain size dependent, i.e. grain growth dominates as the grain size is below a critical value.

The main disadvantage of the precipitated powder is often due to the presence of hard agglomerates that result in heterogeneous density throughout the green compact. This, in turn, results in differential densification during sintering, and in stable residual pores. Differential densification of ultrafine zirconia alloys during sintering was very well described by van de Graaf *et al.*,[15] who characterised the microstructure evolution and followed the pore and grain size and their distributions with sintering pressure and temperature. The small and dense particle aggregates, often with necks formed during the calcination, sinter already during the heating stage. However, the local density between these aggregates is much lower with a fewer contact points per unit volume. As a result of the pore volume transfer from the denser aggregates to their less dense peripheral regions, the latter do not undergo densification at the same temperatures. This type of differential densification may lead to conditions where the dense aggregates undergo full densification while the total volume shrinkage of the compact is negligible. These two different stages of the sintering of the primary nanoparticles and the secondary agglomerates in zirconia powder were determined using the shrinkage rate data.[16] Moreover, it was concluded that the full densification of the denser aggregates results in single crystallites due to local grain growth; these crystallites act as precursor grains for abnormal grain growth at higher temperatures. Therefore, in order to preserve the nanocrystalline character during the pressureless sintering, the aggregates' size and distribution should be as small as possible.[17] In this respect, soft agglomerates of zirconia alloy nanopowders (100 nm) compacted up to 340 MPa resulted in green densities up to 47%, but with single pore size of 6·5 nm and narrow pore size distribution.[18] Such compacts needed prolonged sintering of 80 to 100 h below 1000°C in order to achieve near full density and yet preserve the nanocrystalline character.

In contrast, the agglomerate free spherical shape particles are more advantageous for the fabrication of homogeneous green compacts. The spherical particle morphology is also important for decreasing the interparticle frictional forces during the pressure assisted densification. However, most of the dry pressing techniques lead to heterogeneous density within the green compact due to the frictional forces between the particles. Application of critical pressure (higher than the agglomerate strength) to nanocrystalline compacts during cold isostatic pressuring (CIP) was found to improve the homogeneity in the green density.[15,19] The effect of the particle size distribution on sintering of ceramic particles was modelled and experimentally studied.[20–23] The densification rate before grain growth was maximal for particles with wide particle size distribution.[20] However, while considering grain growth, the densification rate was found to decrease with increase in the width of the starting particle size distribution. The resultant grain size – density trajectory exhibited the advantage of the narrow particle size distribution on preservation of the fine grain size at full densification.[21] Fine and uniform particle size alumina powder compact was found to prolong the intermediate stage of sintering during which sintering proceeded with negligible grain growth.[22] This finding is in agreement with the theoretical expectation where wide
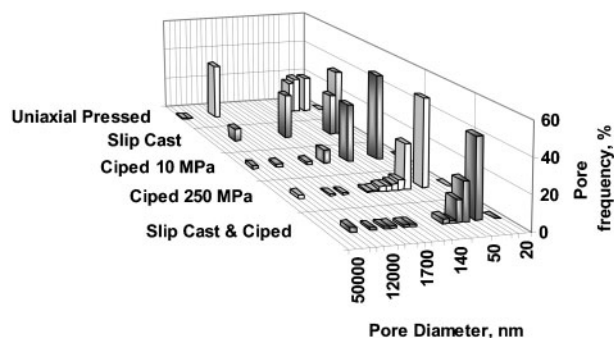
2 Pore size distribution determined by mercury porosimetry in 34 nm YAG nanoparticle green compacts: systematic decrease in fraction of larger pores is observed by moving from uniaxial pressing to slip casting, CIP with increased applied pressures and ciped slip cast

particle size distribution may enhance particle coarsening due to inhomogeneous dihedral angles between the nanoparticles.[23]

On the other hand, homogeneity of the green density may be increased by wet processing of the nanocrystalline powder (i.e. slip casting, spin and dip coating, pressure filtration, etc).[24,31,32] The similar effect is expected for application of very high pressures.[33–35] Application of 800 MPa uniaxial pressure to 5 nm zirconia nanocrystalline powders, formed by chemical vapour synthesis, resulted in green densities around 55%. Such compacts were already transparent in the green state, and fully sintered to transparent solids at temperatures as low as 950°C for 1 h in vacuum.[35] Green compacts of nanocrystalline Y-TZP powders from different sources and with various grain sizes were prepared by CIP between 300 MPa and 1 GPa.[36] Homogeneous green bodies with average pore diameter smaller than 10 nm could be pressureless sintered to full density while preserving the nanograin size. The need to minimise the pore size was clearly shown for full densification to optical transparency.[37] Effects of CIP and slip casting on the particle packing of nanocrystalline transition alumina were compared.[38] Slip cast compacts exhibited higher homogeneity of particle packing compared to the ciped compacts. This was attributed to the optimal dispersing of the particles in the slurry before slip casting.

Systematic decrease in the volume of the larger pores in the green compact of 34 nm spherical YAG (yttrium aluminum garnet) nanoparticles was observed by the application of either uniaxial pressing, slip casting, CIP at increasing pressures, or CIP of the slip cast compact (Fig. 2).

Microwave sintering was also used for the densification of gas condensation synthesised nanocrystalline γ–alumina particles.[39] However, the accompanied volume change, due to the polymorphic phase transformation, resulted in porous compacts. Recently, microwave sintering was applied to different nanocrystalline oxides resulting in near full density nanocrystalline ceramics.[40,41] Microwave–laser hybrid process was used for the sintering of 23 nm nanocrystalline zirconia alloy particles (and agglomerate size of 210 nm) to near full density within 3 min at ~1700°C.[40] Sintering of a similar powder by microwave heating only, necessitated longer durations

of 20 to 30 min at the sintering temperatures 1500 and 1400°C respectively. Nevertheless, the grains grew to the submicrometre size.[41]

Another approach to inhibit the coarsening of the nanoparticles during the heating is to shorten the heating time by rapid heating.[42–49] Based on the rate equations for densification and grain growth, Brook and coworkers[42,43] used fast firing for rapid densification of α-alumina and BaTiO₃ at temperatures higher than their conventional sintering temperatures. However, the mechanism for the measured grain growth could not clearly be determined and was believed to be surface diffusion. Non-agglomerated nanocrystalline Y-TZP with 22 nm particle size was pressed at 100 MPa and rapidly heated at 500 °C/min to 1300°C.[44,45] Extremely short heating duration of 1 min enabled near full density with final grain size of 100 nm. However, the disc shape specimens were very thin (1 × 10 mm²) and the homogeneity of the final density was not shown. Similar work on nc-Y-TZP (yttria stabilised tetragonal zirconia polycrystals), albeit with lower heating rates up to 200 °C/min, has demonstrated the opposite trend by which densification was retarded by the fast heating rates, and the grain growth was unaffected.[46] Based on the observed microstructure, the differential densification was related to thermal gradients in the nanocrystalline compact. Therefore, while the compact external surfaces are rapidly heated to the sintering temperature, the internal regions are at lower temperatures. Rapid densification of the external regions leads to the formation of dense regions with decreasing thermal conductivity; that, in turn, inhibits heat transfer which is needed for the densification of the internal regions. This specimen size effect is a drawback in the application of the rapid heating technique to engineering articles with a few millimetres in size. Differential densification was also confirmed by rapid rate sintering of nanocrystalline indium tin oxide (ITO) between 1300 and 1600°C.[47] A two step sintering regime with a rapid heating rate was suggested by Chen and Wang to preserve the nanocrystalline character of the original powder compact.[48–50] A modified version of the rapid rate sintering was applied to nanocrystalline barium titanate ceramics filter pressed and ciped to yield green density of 55%.[51] The combined rapid rate sintering, rate controlled sintering and two stage sintering has led to the slowest grain growth rate at all densities measured during the densification. Recently, 99% dense nanocrystalline Y-TZP with 65 nm average grain size was fabricated using the hybrid two stage conventional/microwave sintering approach for slip cast compacts.[52,53]

It turns out that increase in the heating rate to the sintering temperature only, may not suffice for the rapid and homogeneous densification of nanocrystalline ceramic compacts during the pressureless sintering. In this respect, the application of pressure at the sintering temperature by hot pressing (HP), hot isostatic pressing (HIP), and sinter forging (SF), as well as the simultaneous rapid heating rate during spark plasma sintering (SPS), is useful as will be discussed below.
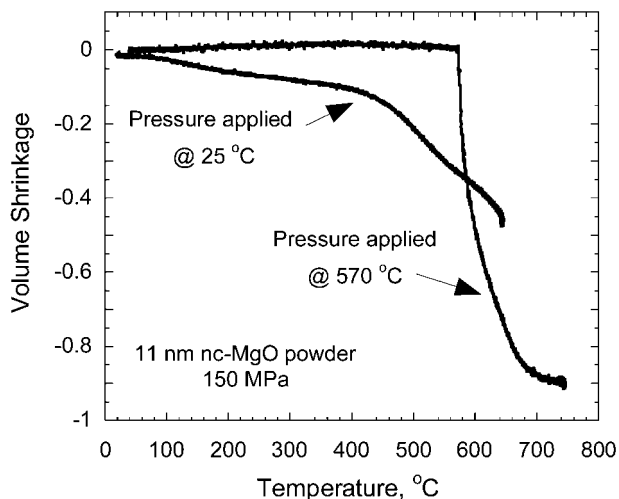
Application of pressure

Analyses of the microstructure evolution during the pressureless sintering of many nanocrystalline systems indicate that inevitable grain growth occurs, especially at the final stage of sintering. This arises due to the curvature driven diffusional process at the grain boundaries where the isolated pores are no more efficient to pin the grain boundaries. Consequently, the application of pressure already at low temperatures has been adopted in various manners such as hot pressing (HP), hot isostatic pressing (HIP), and sinter forging (SF) for time independent densification processes such as plastic deformation as well as time dependent diffusional processes active at low temperatures.

Hot pressing of ultrafine ceramics by pressure calcination to ultrafine grain ceramics is known for more than 40 years.[54,55] The application of pressure during the sintering of nanocrystalline ceramics leads to various mass transport mechanisms such as plastic yield, diffusion controlled creep, and grain boundary sliding.[56,57] Important aspects in the pressure application are the pressure type (shear, hydrostatic), its level and the regime at which it is applied. Molecular dynamic simulation of the pressure assisted sintering revealed that both hydrostatic and uniaxial loadings accelerate the densification process in nanocrystalline copper.[58] However, the uniaxial load was more effective due to the grain boundary sliding caused by shear stresses. In this respect, fully dense nanocrystalline Y-TZP with 45 nm grains were fabricated using pressureless sintering at 1100°C followed by HIP at 1250°C for 2 h while using glass cladding.[59]

Green bodies of nanocrystalline γ-alumina were compacted at high pressures up to 5 GPa followed by pressureless sintering between 1000 and 1600°C.[60] It was found that specimens compacted above 3 GPa reached near theoretical density and retained their nanocrystalline character (average grain size of 150 nm). Below 3 GPa, transformation to α-alumina was accompanied by the formation of porous vermicular structure between 1000 and 1150°C leading to porous sintered microstructure. Similar studies by Gallas *et al.*[61] and Mishra *et al.*[62] led to fully dense nanocrystalline alumina specimens with the average grain size of 190 nm.

Densification of ultrafine and nc-MgO by hot pressing was thoroughly investigated.[54,63–67] Pressure calcination of Mg(OH)₂ powders at 1000°C and 46 MPa resulted in fully dense MgO specimens albeit with micrometre grains.[54] The effect of the particle size in the range of 10 to 260 nm on the densification and grain growth behaviour was investigated using nc-MgO formed by vapour phase oxidation. These were hot pressed between 900 and 1300°C at 30 MPa in N₂ atmosphere.[63] At lower temperatures, sintering of the primary particles within the agglomerates as well as rearrangement of the agglomerates takes place. Between 900 and 1100°C, grain growth is controlled by pore mobility, while around 1300°C rapid grain growth occurs. The submicrometre grain size was obtained only in the compacts hot pressed for 1 h below 1100°C. The transluscent specimen with 99·7% maximal density was obtained using the optimal primary particle size of 44 nm. This particle size effect was related to the soft nature of the agglomerates. Nanocrystalline MgO with 11 nm particle size was also hot pressed at lower temperatures ranged 700–800°C under 100–200 MPa.[64] It was found that the temperature at which the pressure is applied during the heating strongly affects the maximum shrinkage rate (Fig. 3) as well as the overall shrinkage at the hot
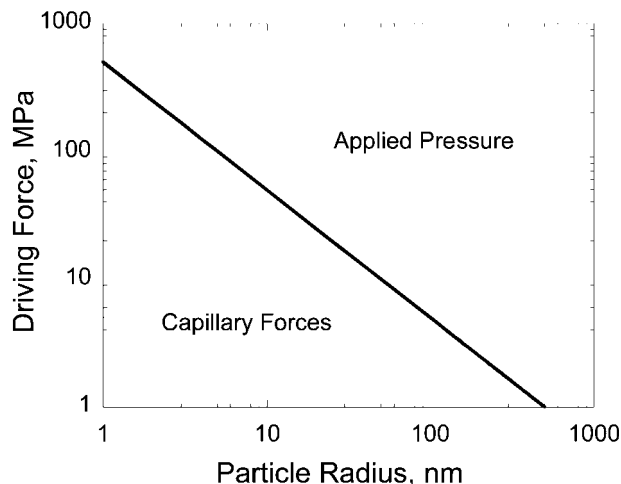
3 Volume shrinkage during hot pressing of nanocrystalline MgO powder showing effect of pressure application regime on total shrinkage

4 Driving force versus particle size diagram showing dominating range of applied pressure with respect to original particle size: line represents decay in sintering driving force due to capillary forces as initial particle size increases

pressing temperature. This effect was related to the change in the particle morphology due to the plastic deformation during the heating. Densities higher than 99·5% with average grain size of 73 nm were achieved by 30 min hot pressing at 790°C and 150 MPa.

The relative contributions of the applied pressure and the capillary forces to the driving force for sintering may be expressed by[65]

$$P = P_{Applied} + \frac{2\gamma_{SV}}{r} \qquad (3)$$

where γ_{SV} is the solid vapour surface energy per unit area and r is the particle radius. An average value of this surface energy term for ionic crystals is ~1 J m^{-2}. Using equation (3), the dominating range of the applied pressure with respect to the original particle size is shown in Fig. 4. The line represents decay in the sintering driving force due to the capillary forces as the initial particle size increases. Therefore, for a given particle size, the threshold pressure exists above which the pressure is an effective driving force for densification.[66] High applied pressure is beneficial both

at the first and intermediate stages of sintering through different densification mechanisms: nanoparticle rearrangement, plastic deformation, particle sliding and pore shrinkage.

These latter processes also decrease the relative density of the available particle surfaces and their corresponding contributions to the particle coarsening by surface diffusion. However, towards the final stage of sintering, when continuous pores convert to isolated pores, the applied (shear) pressure acts as a driving force for grain growth by increasing the vacancy concentration gradient across the grain boundary.[67] Pressures comparable to the nanoparticle yield strength at the hot pressing temperature should suffice for rapid densification by plastic deformation and particle sliding. In this respect, increase in the hot pressing pressure between 100 and 200 MPa applied at 550°C during the heating exhibited a negligible effect on the densification of nc-MgO compacts (Fig. 5a). This most possibly is due to the low yield strength of MgO single crystals at this temperature (Fig. 5b), compared to the applied
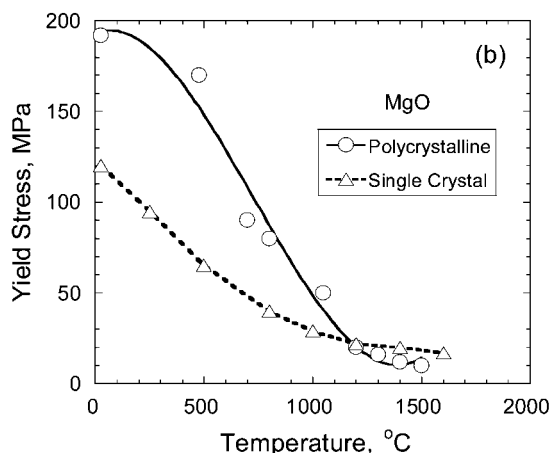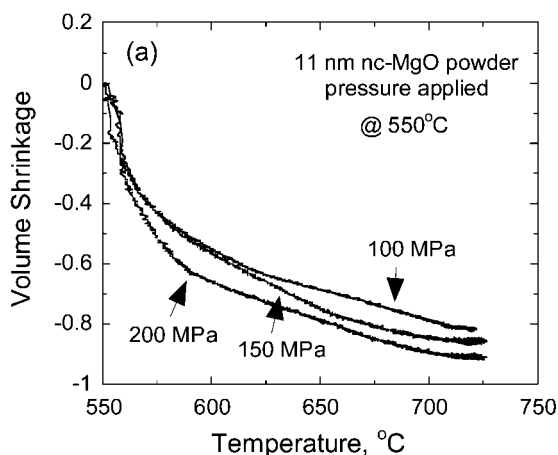
5 *a* volume shrinkage during hot pressing of nc-MgO powder at different pressures applied at 550°C proceeds by plastic deformation: negligible effect of pressure on densification is due to low yield stress in *b* compared to applied pressure at corresponding hot pressing temperature

pressures. Rapid densification immediate to the pressure application points to time independent processes that take place such as plastic yield or particle rearrangement and sliding in porous compact. The latter mechanism may involve diffusional processes, however, with fast kinetics as expected for surface diffusion.

The effect of the applied pressure and the particle size (12 to 70 nm) on the densification mechanism during the hot pressing of nc-TiO$_2$ (anatase) was investigated.[68–70] The activation energies determined from the shrinkage data for the smallest initial particle size of 12 nm were almost constant with the applied pressure in the 125–600 MPa range. This was interpreted as a single densification mechanism such as superplastic deformation operative at the smallest particle size. However, at the largest particle size of 70 nm, significant changes in the activation energy were observed at different temperature ranges, and related to plastic deformation and diffusional processes aided by surface diffusion.

Another form of pressure application, intended to enhance densification and retain the nanocrystalline character in the dense ceramic, is by sintering forging.[71–76] The strain rates during the sinter forging of nanocrystalline oxide powders depend on the applied stress, but typically are of the order of the creep rates, i.e. 10^{-3}–10^{-6} s^{-1}. The lack of constrain around the specimen differentiates this technique from the regular hot pressing methods. The early experiments were performed on nanoparticles formed by inert gas condensation (IGC).[70,75] Sinter forging of 12 nm TiO$_2$ particles at temperatures below 0·5 Tm enabled densities up to 97% and a grain size of 60 nm.[75] However, extremely high pressure of 2 GPa at 350°C was first used for the green compaction to 70% density, followed by two step sinter forging at 57 and 93 MPa at 650°C for 1 h. Analysis of the creep data during the sinter forging was in agreement with densification due to the grain boundary sliding. Recently, similar anatase TiO$_2$ nanopowders were synthesised by the sol–gel method (7 to 38 nm), and uniaxial cold compaction at 920 MPa resulted in green densities up to 64% with the coarser particles.[71] The maximum density of 95% with a grain size of 135 nm was reached by pressureless sintering of the 15 nm particles at 1000°C and 500 MPa. The densification was considered to be aided by the anatase to rutile phase transformation.

Sinter forging of nc-zirconia formed by IGC with 6 nm initial particles, for 3 h at 300 MPa and 950°C led to almost fully dense specimens with the average grain size of 45 nm.[66] Nanocrystalline Y-TZP powder with 15 nm particles was synthesised by wet precipitation, and was both pressureless sintered and sinter forged at different conditions.[74] Pressureless sintering between 1050 and 1200°C resulted in densities up to 90% with a grain size of ~120 nm. In comparison, sinter forging of the same powder at the highest strain rate (2×10^{-3} s^{-1}) and 1100°C for 1 h resulted in densities up to 98% with the similar grain size. Densification of the compact was related to the elimination of the large and small pores by plastic deformation and diffusion respectively. At the final stage of sintering, accelerated grain growth was observed. High strain rates were believed to assist the final nanocrystalline character before the dynamic grain growth. This expectation modelled and explained in terms of the high density of small pores that left for grain growth inhibition during the intermediate stage and shorter durations available for grain growth.[74] Presintering followed by sinter forging of larger Y-TZP particles of 180 nm between 1300 and 1400°C resulted in densities up to 98% and the submicrometre size grains (300 to 350 nm).[75] Application of 28–84 MPa pressure to the similar nanocrystalline Y-TZP powders at 1100°C was found to reduce the sintering time by a factor of 20–600, compared to the pressureless sintering, for an intermediate density (84%) to be reached.[76] Analysis of the densification and creep data during the sinter forging of nanocrystalline Y-TZP powder compacts was consistent with interface reaction controlled processes.[76,77]

Densification of nanocrystalline alumina by sinter forging was investigated using transition aluminas.[78–80] Transformation from transition aluminas to stable α-alumina is accompanied by the volume decrease and results in porous vermicular structure during the pressureless sintering. Seeds of α-alumina were added to the nanocrystalline transition γ-alumina followed by sinter forging at 1250°C and 79 MPa, which resulted in transparent α–alumina with submicrometre grain size.[78] Similar α–seeding of the transition θ-alumina decreased the transformation temperature, hence enhanced the densification by sinter forging during the transformation.[79] Densities as high as 99·7% with a grain size of 230 nm were reached at 1060°C and 235 MPa for 30 min. It was deduced that soft agglomerate obtained by ethanol dispersion contributed to the homogeneous green microstructure and in turn to higher final density, compared to water dispersed powders.[80] Nevertheless, the extent of the grain growth and the loss of the nanostructure depended on the sinter forging temperature.

Spark plasma sintering

As was shown above, high heating rates, applied pressure, and strain rates, each enhances the densification process of nanocrystalline powder compacts. Spark plasma sintering (SPS), or field assisted sintering (FAS) combines these latter processing parameters needed for efficient densification of nanocrystalline compacts. Spark plasma sintering is a hot pressing technique where very high heating rates (~500 °C/min) were achieved by the application of pulsed electrical current and simultaneous loading. These sintering conditions lead to superfast densification of nanocrystalline powder compacts (within a few minutes) and to retention of the nanostructure. This technique was found to be especially compatible for the densification of nanocrystalline powders.

Many atomic transport mechanisms may be active during the sintering and densification of nanocrystalline oxide powders. Neglecting the evaporation–condensation and viscous sintering mechanisms that are limited to specific material systems, the main transport mechanisms are surface, grain boundary, and lattice diffusion. While surface diffusion during pressureless sintering can change the pore shape, the corresponding pore volume is barely affected. Consequently, mass transport by surface diffusion is not considered as a densification mechanism. This no more holds for densification via SPS. The main advantage of the SPS is due to the preservation of the particle specific surfaces during heating. Under applied load, the compact densification may benefit from the

low temperature mass transport mechanisms provided by the nanoparticle surfaces and interfaces. The short sintering durations at low temperatures are expected to limit the diffusion controlled grain growth.

Spark plasma sintering was used for the densification of different monolithic nanocrystalline oxides, including TiO₂,[81,82] Al₂O₃,[83–90] MgO,[91,92] ZnO,[93,94] ZrO₂,[95–100] BaTiO₃[90,101–105] as well as oxide nanocomposites,[106–109] and ferroelectric/dielectric multilayers.[110] Nanocrystalline TiO₂ with 20 nm particle size was spark plasma sintered for 1 h at 62 MPa between 600 and 800°C, using the heating rate of 150 °C/min and current density 1273 [A/cm²].[81] Dense specimens up to 99% and nanometric grains of 200 nm were formed by 1 h SPS at 700°C. For comparison, pressureless sintering for 1 h at 900°C resulted in fully dense specimens with average grain size larger than 1 μm. Comparison between the densification rates revealed a decrease of 200°C in the corresponding sintering temperatures by SPS.

As was mentioned previously, densification of nanocrystalline transition alumina is very difficult due to the phase transformation accompanying the densification. Comparative work by Mukherjee and coworkers[83–85] has shown better sintering behaviour of the stable α–alumina compared to transition γ–alumina during the SPS. Nevertheless, nanocrystalline γ-alumina powder with 50 nm average particle size was densified at 1400°C and 100 MPa with no holding time to 99·9% density and average grain size of 300 nm.[86] Wang *et al.*[87] showed that increase in the alumina particle size into the micrometre range significantly decreased the powder sinterability by SPS. Submicrometre size alumina particles were successfully sintered to dense monolithic and composite specimens, however at the conventional sintering temperatures (i.e. above 1650°C).[88,89] Shen *et al.*[90] used submicrometre size pure and MgO doped alumina powders at various SPS conditions. Using 200 MPa at 1150°C, 99·2% dense alumina with 600 nm average grain size were fabricated. Higher densities were also achieved albeit with larger grain size.

Nanocrystalline 11 nm MgO particles were densified to full density using two step SPS for 3 min at 450°C, followed by 5 min at 825°C and 150 MPa.[91] The resultant specimens were optically transparent with an average grain size of 42 nm. The rapid densification and limited grain growth during the SPS may be related to the grain boundary sliding of the nanoparticles. Densification maps of nc-MgO, based on the hot isostatic pressing model, showed significant contribution by the plastic deformation to immediate densification at the corresponding SPS temperatures.[92] Further densification accompanied by grain growth then occurred by grain boundary diffusional processes.

Agglomerate free nanocrystalline ZnO powders with 20 nm particle size were formed by precipitation from salt solutions and subjected both to pressureless sintering and SPS.[93,94] The nanopowder was uniaxially pressed at 50 MPa within the graphite die which was heated between 400 and 750°C for 2 min in the SPS vacuum. For comparison, pressureless sintering was performed on the 300 MPa ciped green compacts for 2 h between 800 and 1200°C at the heating rate of 5 °C/min. The density of the SPS specimens varied between 96 and 98% with the maximum at 550°C. The grain size of the

spark plasma sintered specimens was ~100 nm below 550°C and similar to that of pressureless sintered specimens at 800°C. However, enhanced grain growth was observed above 550°C. The grain size was also found to increase with the pressureless sintering temperature, especially at 1200°C (5 to 8 μm). More important was the maximal photoluminescence intensity at the green emission observed from the 550°C SPS specimen compared to those from the sintered specimens.

Nanocrystalline BaTiO₃ and other ferroelectric oxides were spark plasma sintered at different conditions to form fully dense compacts with different grain sizes in the nanometre range.[90,101–105] Zhao *et al.*[86] used 36 nm BaTiO₃ particles and a high heating rate of 200 °C/min at 50 MPa and 820°C for 3 min to reach 98% dense specimens with 60 nm grain size. Li *et al.*[101, 102] used 20 nm BaTiO₃ particles for SPS densification at different SPS conditions. Varying the heating rate between 50 and 250 °C/min did not change the final grain size of ~300 nm in the specimens sintered for 1 min at 40 MPa and 920°C. However, the heating rate of 400 °C/min at the same SPS conditions resulted in finer grain size of 250 nm. Spark plasma sintering at different sintering temperatures, between 800 and 1300°C, resulted in partially dense specimens with nanocrystalline (<50 nm) grain size below 1050°C, and submicrometre grain size above 1050°C.[101] The change in the grain growth rate was found to strongly depend on both the SPS duration and temperature. For comparison, pressureless sintering at similar SPS temperatures resulted in densities lowered by 20 to 30% and grain sizes larger by a factor of 2.

Zhao *et al.*[104] also used 30–40 nm nanoparticles to form dense and nanocrystalline BaTiO₃ compacts. Spark plasma sintering was performed at 100 MPa for 2 to 5 min within the temperature range of 800–1000°C, using the heating rate of 200°C/min. The specimens were finally polished and air annealed between 700 and 800°C to relieve the residual stresses as well as the elimination of excess oxygen vacancies. Both groups investigated the effect of the final grain size in the 50–1200 nm range on the dielectric properties of BaTiO₃.[102, 104] Decrease in the grain size led to significant decrease in the Curie temperature, as well as to disappearance of ferroelectricity as an intrinsic size effect. However, dense nanocrystalline BaTiO₃ with a grain size between 20 and 100 nm exhibited remnant polarisation which indicates the preservation of the ferroelectric properties within the 20 nm grains.[103]

The possibility to form fully dense oxides with nanometric grain size depends on the management of the competitive thermal processes involved in SPS. Nanocrystalline MgO compact, confined within a graphite die and subjected to uniaxial pressing, was assumed to behave as a liquid and experience hydrostatic stress components. Therefore, an appropriate hot isostatic pressing (HIP) model was successfully used for the description of the densification behaviour of the ceramic nanopowder.[92] Based on the HIP equations, the densification of nanoparticle green compact, which is rapidly heated and subjected to applied pressure, may be described as follows: some particle coarsening is expected during the heating up, due to the fast kinetics of the surface diffusion. The smaller is the nanoparticle size, the higher is the driving force for coarsening, and the faster is
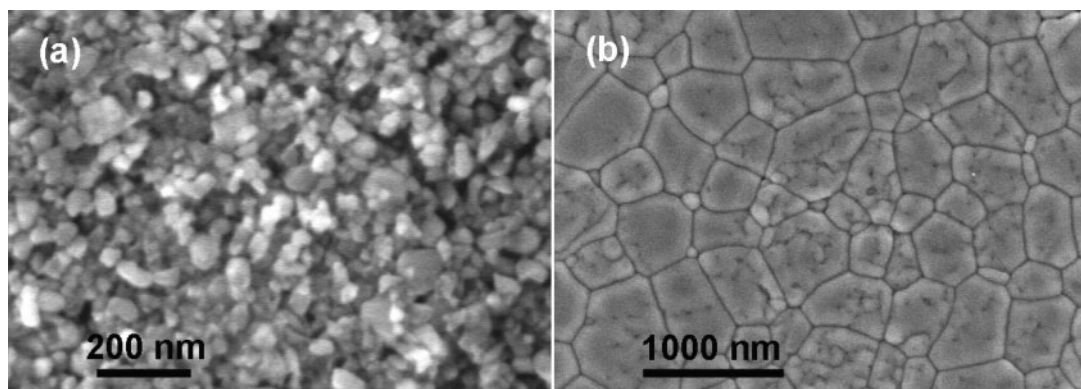
a 11 nm MgO nanoparticles densified by plastic deformation during 5 min at 100 MPa and 775°C; *b* 34 nm YAG nanoparticles densified by grain boundary sliding aided by liquid phase during 5 min at 150 MPa and 1400°C; nanostructure is preserved in *a* but lost in *b*

6 HRSEM images showing fully dense structures formed by SPS

the coarsening kinetics. However, two distinct states may exist with respect to the applied pressure.

(i) First if the applied pressure exceeds the corresponding yield strength of the nanoparticles during the heating, immediate densification proceeds by the plastic deformation. This time independent densification may cease when the neck area between the grains grows, so that the applied pressure decreases below the yield strength. In this case, the residual pores are distributed homogeneously along the grain boundaries and grain junctions, and the average pore size is expected to be far smaller than the average grain size. The relative density of the nanocrystalline green compacts often varies between 30 and 60%, depending on the powder characteristics. Therefore, densification by plastic deformation may increase the relative density into the intermediate stage of sintering (up to 85%) when continuous pores convert to closed pores. At this stage, the densification rate is much higher compared to the grain growth rate, thus preserving the fine grain size. As an example, the nanostructure in dense nc-MgO that corresponds to such a process is shown in Fig. 6*a*. At the final stage of sintering, further densification for the removal of the isolated pores is accompanied by curvature driven grain boundary diffusion which becomes active at higher temperatures. At this stage, the isolated pores are less efficient in pinning the grain boundaries towards the grain growth. While grain growth proceeds by the atomic jump perpendicular to the gb, the densification by pore removal proceeds by atomic diffusion along the gb's. Therefore, the densification rate reverses, and is lower compared to the grain growth rate. Consequently, as was shown by Shen *et al.*[95,99] an SPS temperature for the maximal shrinkage rate exists; above this temperature enhanced grain growth may take place. This temperature was found to depend on the powder characteristics as well as on the heating rate and the applied pressure. The optimal SPS temperatures for 0·4 μm α-alumina powder were 1130 and 1070°C at 50 and 100 MPa respectively, almost irrespective of the heating rate.[89] On the other hand, combined effects of the heating rate (100 and 200 °C/min) and applied pressure (10 and 50 MPa) significantly changed the optimal SPS temperature within the 950–1370°C temperature range, when nanocrystalline γ-alumina was used.[90]

(ii) On the other hand, if the applied pressure is not sufficient to produce plastic deformation of the nanoparticles during heating, densification may proceed by particles sliding aided by surface diffusion. In porous green compact, nanoparticles may slide over each other to form denser compact. However, further densification to higher densities at low temperatures may be similar to the deformation of granular compacts, where polyhedral shape clusters of nanoparticles/nano-grains slide over each other together with the sliding of single particles/grains.[111–113] A similar microstructural effect was observed due to cooperative grain boundary sliding during the uniaxial compression of nanocrystalline Y-TZP containing a glassy phase.[113] Densification of the nanograins by the sliding of single nanograins over each other is possible in the porous compacts as shown for 18 nm Y_2O_3 nanoparticles (Fig. 7*a*). Nevertheless, when some level of density is reached, further sliding of single grains over each other necessitates extremely high activation energy due to the high density of interfaces formed. Therefore, the formation of nanoparticle clusters and their mutual sliding is energetically favoured (Fig. 7*b*). As a result, relatively dense clusters of nanoparticles form during the intermediate stage of sintering. These clusters resemble the final grains, but they contain subgrains separated by low angle grain boundaries (LAGB's). Such clusters meet each other at high angle grain boundaries (i.e. Fig. 7*c*). As the temperature is further increased, coarsening may take place both at the subgrain and the grain level. At the final stage of sintering, where grain boundary- and lattice-controlled diffusional processes dominate, full densification and grain growth are accompanied by subgrain rotation and diffusion-out of the internal LAGB's, as well as curvature driven grain growth (i.e. Fig. 7*d*).
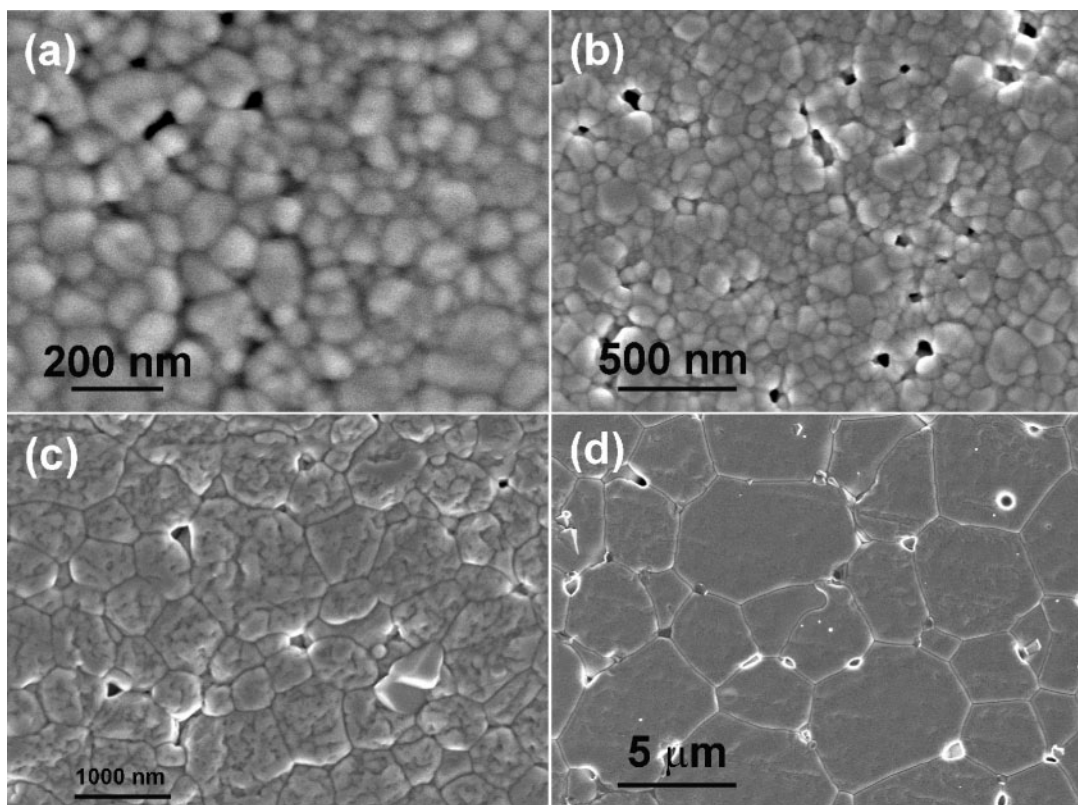
a densification by nanoparticles sliding and coalescence in porous compact at 1100°C; *b* formation of nanograin clusters at 1300°C; *c* growth of clusters by their sliding, rotation and coalescence at 1400°C; *d* curvature driven grain growth at 1500°C

7 HRSEM images exhibiting microstructure evolution and grain growth during densification of 18 nm Y_2O_3 nanoparticles by SPS

Although the exact nature of the rapid densification during the SPS is still under debate, a general agreement exists about the enhanced rates of the diffusion controlled processes involved. Densification of nanocrystalline yttrium aluminum garnet (YAG) nanoparticles by SPS resulted in fully dense transparent oxides with micrometre size grains.[114,115] Analysis of the grain growth data at different SPS temperature ranges and its comparison to the grain growth data in YAG revealed more than one order of magnitude increase in the grain growth rate. The diffusivity and activation energies determined from the grain growth data at the lower SPS temperatures were in agreement with the formation of a liquid layer at the nanoparticle surfaces that enabled enhanced densification and grain growth through the liquid film. At higher SPS temperatures (i.e. above 1400°C), grain growth was in agreement with normal grain growth from the literature. These observations indicated that under certain circumstances particle surfaces may soften under the SPS conditions at low temperatures.[115] This effect leads to enhanced densification and grain growth via grain sliding, rotation and gb migration within the clusters, hence to the loss of the nanocrystalline character. Alternatively, if no surface softening occurs during the rapid heating, surface diffusion will dominate at lower temperatures, as is necessary for densification with limited grain growth. The observed microstructure evolution during the SPS of oxide nanoparticles clearly demonstrates the need for long term low temperature processes for full densification with negligible grain growth.

Epilogue

The art and science of sintering and densification of ceramic nanoparticles has reached the stage where fully dense nanocrystalline articles may be fabricated. Oxide nanoparticles with equiaxed morphology and narrow size distribution are necessary for green compacts with homogeneous density and low pore-to-particle-size ratio. The forces acting between the nanoparticles are the first to be controlled, mainly through the liquid medium and/or by the application of high isostatic pressures. Preservation of the nanocrystalline character at full densification should adopt the application of high pressures at minimum temperatures that are necessary for sintering and structural integrity.

Acknowledgements

References

1. A. J. Burggraaf, A. J. A. Winnubst and H. Veweij: in 'Third Euroceramics', (eds. P. Duran and J. F. Fernandez), Vol. 3, 561–576; 1993, Spain, Faenza Editrice Iberica S.L.
2. A. C. F. Cocks: *Acta Metall. Mater.*, 1994, **42**, 2191–2210.
3. R. A. Andrievski: *J. Mater. Sci.*, 1994, **29**, 614–631.
4. J. R. Groza and R. J. Dowding: *NanoStruc. Mater.*, 1996, **7**, 749–768.

5. M. J. Mayo: *Inter. Mater. Rev.*, 1996, **41**, 85–115.
6. W. D. Kingery and B. Francois: in 'Sintering and related phenomena', (eds. G. C. Kuczynski, N. A. Hooton and C. F. Gibbon), 471–498; 1967, New York, Gordon and Breach.
7. M. J. Bannister: in 'Sintering and related phenomena', (eds. G. C. Kuczynski, N. A. Hooton and C. F. Gibbon), 581–605; 1967, New York, Gordon and Breach.
8. E. B. Slamovich and F. F. Lange: *J. Am. Ceram. Soc.*, 1993, **76**, 1584–1590.
9. A. Akash and M. J. Mayo: *J. Am. Ceram. Soc.*, 1999, **82**, 2948–2952.
10. F. Wakai, T. Akatsu and Y. Shinoda: *Acta Mater.*, 2006, **54**, 793–805.
11. W. Y. Shih, W-H. Shih and I. Aksay: *J. Mater. Res.*, 1995, **10**, 1000–1015.
12. E. Matijevic: in 'Ultrastructure processing of advanced ceramics', (eds. J. D. Mackenzie, and D. R. Ulrich), 429–442; 1988, New York, Wiley.
13. J.-G. Li, T. Ikegami, J.-H. Lee and T. Mori: *Acta Mater.*, 2001, **49**, 419–426.
14. C. Ho, J. C. Yu, T. Kwong, A. C. Mak, and S. Lai: *Chem. Mater.*, 2005, **17**, 4514–4522.
15. M. A. C. G. van de Graaf, J. H. H. Ter Maat and A. J. Burggraaf: *J. Mater. Sci.*, 1985, **20**, 1407–1418.
16. G. S. A. M. Theunissen, A. J. A. Winnubst and A. J. Burggraaf: *J. Eur. Ceram. Soc.*, 1993, **11**, 315–324.
17. J. Xing-Xiang, H. Dong-Shen, and W. Luqian: *J. Mater. Sci.*, 1994, **29**, 121–124.
18. P. Duran, M. Villegas, F. Capel, J. F. Fernandez and C. Moure: *J. Mater. Sci.*, 1997, **32**, 4507–4512.
19. M. T. Tsai and H. C. Shih: *J. Mater. Sci.*, 1993, **28**, 4530–4535.
20. J.-M. Ting and R. Y. Lin: *J. Mater. Sci.*, 1994, **29**, 1867–1872.
21. J.-M. Ting and R. Y. Lin: *J. Mater. Sci.*, 1995, **30**, 2382–2389.
22. F.-S. Shiau, T.-T. Fang and T.-H. Leu: *J. Am. Ceram. Soc.*, 1997, **80**, 286–290.
23. R. M. Cannon and W. C. Carter: *J. Am. Ceram. Soc.*, 1989, **72**, 1550–1555.
24. X. Yang and M. N. Rahaman: *J. Eur. Ceram. Soc.*, 1997, **17**, 525–535.
25. D.-J. Chen and M. J. Mayo: *NanoStruct. Mater.*, 1993, **2**, 469–678.
26. G. Skandan, H. Hahn, M. Roddy and W. R. Cannon: *J. Am. Ceram. Soc.*, 1994, **77**, 1706–1710.
27. A. P. Hynes, R. H. Doremus and R. W. Siegel: *J. Am. Ceram. Soc.*, 2002, **85**, 1979–1987.
28. S.-J. L. Kang and Y.-I. Jung: *Acta Mater.*, 2004, **52**, 4573–4578.
29. M. N. Rahaman: 'Ceramic processing and sintering', 602–610; 2003, New York, Marcel Dekker.
30. S-J. L. Kang: 'Sintering, densification, grain growth and microstructure', 153–160; 2005, Amsterdam, Elsevier.
31. H. Vesteghem, A. Lecomte and A. Dauger: *J. Non-Cryst. Solids*, 1992, **147&148**, 503–507.
32. Y. Hirata, M. Nakamura, M. Miyamoto, Y. Tanaka and X. H. Wang: *J. Am. Ceram. Soc.*, 2006, **89**, 1883–1889.
33. V. V. Srdic, M. Winterer and H. Hahn: *J. Am. Ceram. Soc.*, 2000, **83**, 729–736.
34. Y. Jorand, M. Taha, J. M. Missiaen and L. Montanaro: *J. Eur. Ceram. Soc.*, 1995, **15**, 469–477.
35. H. Hahn, J. Logas and R. S. Averback: *J. Mater. Res.*, 1990, **3**, 609–614.
36. M. Trunec and K. Maca: *J. Am. Ceram. Soc.*, 2007, **90**, 2735–2740.
37. A. Krell and J. Klimke: *J. Am. Ceram. Soc.*, 2006, **89**, 1985–1992.
38. M. Azar, P. Palmero, M. Lombardi, V. Garnier, L. Montanaro, G. Fantozzi and J. Chevalier: *J. Eur. Ceram. Soc.*, 2008, **28**, 1121–1128.
39. J. Freim, J. McKittrick, J. Katz and K. Sickafus: *NanoStruc. Mater.*, 1994, **4**, 371–385.
40. R. Peelamedu, A. Badzian, R. Roy and R. P. Martukanitz: *J. Am. Ceram. Soc.*, 2004, **87**, 1806–1809.
41. C. Garcia-Ganan, J. J. Melendez-Martinez, D. Gomez-Garcia and A. Dominguez- Rodriguez: *J. Mater. Sci.*, 2006, **41**, 5231–5234.
42. M. P. Harmer and R. J. Brook: *J. Brit. Ceram. Soc.*, 1981, **80**, 147–148.
43. H. Mostaghaci and R. J. Brook: *J. Brit. Ceram. Soc.*, 1981, **80**, 148–149.
44. C. Feng, H. Qiu, J. Guo, D. Yan and W. A. Schulze: *J. Mater. Synthes. Process.*, 1995, **3**, 25–29.
45. C. Feng, E. Shi, J. Guo, D. Yan and W. A. Schulze: *J. Mater. Synthes. Process.*, 1995, **3**, 31–37.
46. D.-J. Chen and M. J. Mayo: *J. Am. Ceram. Soc.*, 1996, **79**, 906–912.
47. B.-C. Kim, J.-H. Lee, J.-J. Kim and T. Ikegami: *Mater. Lett.*, 2002, **52**, 114–119.
48. I.-W. Chen and X.-H. Wang: *Nature*, 2002, **404**, 168–171.
49. X.-H. Wang, P.-L. Chen and I.-W. Chen: *J. Am. Ceram. Soc.*, 2006, **89**, 431–437.
50. X.-H. Wang, X.-Y. Deng, H.-L. Bao, H. Zhou, W.-G. Qu, L.-T. Li and I.-W. Chen: *J. Am. Ceram. Soc.*, 2006, **89**, 438–443.
51. A. Polotai, K. Breece, E. Dickey, C. Randall and A. Ragulya: *J. Am. Ceram. Soc.*, 2005, **88**, 3008–3012.
52. J. Binner, K. Annapoorani, A. Paul, I. Santacruz and B. Vaidhyanathan: *J. Eur. Ceram. Soc.*, 2008, **28**, 973–977.
53. J. Binner and B. Vaidhyanathan: *J. Eur. Ceram. Soc.*, 2008, DOI: 10.1016/j.jeurceramsoc. 2007, **12**, 24.
54. P. E. D. Morgan and E. Scala: in 'Sintering and related phenomena', (eds. G. C. Kuczynski, N. A. Hooton and C. F. Gibbon), 861–894; 1967, New York, Gordon and Breach.
55. T. Vasilos and E. Rhodes: in 'Ultrafine-grain ceramics', (eds. J. J. Burke, N. L. Reed and V. Weiss), 137–172; 1970, New York, Syracuse University Press.
56. M. G. McKimpson: *Mater. Manufac. Process.*, 1996, **11**, 935–949.
57. R. Suryanarayanan Iyer and S. M. L. Sastry: *Acta Mater.*, 1999, **47**, 3079–3098.
58. H. Zhu and R. S. Averback: *Mater. Sci. Eng. A*, 1995, **A204**, 96–100.
59. R. Chaim and M. Hefetz: *J. Mater. Res.*, 1998, **13**, 1875–1880.
60. E. J. Gonzalez, B. Hockey and G. J. Piermarini: *Mater. Manufact. Process.*, 1996, **11**, 951–967.
61. M. R. Gallas, B. Hockey, A. Pechenik and G. J. Piermarini: *J. Am. Ceram. Soc.*, 1994, **77**, 2107–2112.
62. R. J. Mishra, C. E. Lesher and A. K. Mukherjee: *J. Am. Ceram. Soc.*, 1996, **79**, 2989–2992.
63. K. Itatani, R. Yasuda, F. Scott Howell and A. Kishioka: *J. Mater. Sci.*, 1997, **32**, 2977–2984.
64. D. Ehre, E. Y. Gutmanas and R. Chaim: *J. Eur. Ceram. Soc.*, 2005, **25**, 3579–3585.
65. T. A. Ring: 'Fundamentals of ceramic powder processing and synthesis', 866; 1996, San Diego, Academic Press.
66. G. Skandan, H. Hahn, B. H. Kear, M. Roddy and W. R. Cannon: *Mater. Lett.*, 1994, **20**, 305–309.
67. M. N. Rahaman: 'Ceramic processing and sintering', 515–516; 2003, New York, Marcel Dekker.
68. A. Weibel, R. Bouchet, P. Bouvier and P. Knauth: *Acta Mater.*, 2006, **54**, 3575–3583.
69. S.-C. Liao, K. d. Pae and W. E. Mayo: *NanoStruct. Mater.*, 1995, **5**, 319–325.
70. S.-C. Liao, Y.-J. Chen, W. E. Mayo and B. H. Kear: *NanoStruct. Mater.*, 1999, **11**, 553–557.
71. M. Uchic, H. J. Hoffler, W. J. Flick, R. Tao, P. Kurath and R. S. Averback: *Scripta Met. Mater.*, 1992, **26**, 791–796.
72. J. Li, Y. Ye, L. Shen, J. Chen and H. Zhou: *Mater. Sci. Eng. A.*, 2006, **A390**, 265–270.
73. D. C. Hague and M. J. Mayo: *J. Am. Ceram. Soc.*, 1997, **80**, 149–156.
74. D. C. Hague and M. J. Mayo: *Mater. Sci. Eng. A*, 1995, **A204**, 83–89.
75. C. Barrera-Solano, L. Esquivias and M. Pinero: *J. Eur. Ceram. Soc.*, 1998, **18**, 1429–1438.
76. M. M. R. Boutz, A. J. A. Winnubst, A. J. Burggraaf, M. Nauer and C. Cary: in 'Science and technology of zirconia V', (eds. S. Badwal, J. Bannister and R. Hannink), 275–283; 1993, Lancaster, PA, Technomic Pub. Co.
77. R. Chaim: *J. Mater. Res.*, 1999, **14**, 2508–2517.
78. O.-H. Kwon, C. S. Nordahl and G. L. Messing: *J. Am. Ceram. Soc.*, 1995, **78**, 491–494.
79. C. S. Nordahl and G. L. Messing: *J. Am. Ceram. Soc.*, 1996, **79**, 3149–3154.
80. S. Kwon, C. S. Nordahl and G. L. Messing: *Mater. Manufac. Process.*, 1996, **11**, 969–985.
81. Y. I. Lee, J.-H. Lee, S.-H. Hong and D.-Y. Kim: *Mater. Res. Bull.*, 2003, **38**, 925–930.
82. J. H. Noh, K. S. Hong, H. S. Jung and J-K. Lee: *J. Electroceram.*, 2006, **17**, 913–917.
83. S. H. Risbud, C.-H. Shan, A. K. Mukherjee, M. J. Kim, J. S. Bow and R. A. Holl: *J. Mater. Res.*, 1995, **10**, 237–239.
84. R. S. Mishra, S. H. Risbud and A. K. Mukherjee: *J. Mater. Res.*, 1998, **13**, 86–89.

85. R. S. Mishra and A. K. Mukherjee: *Mater. Sci. Eng. A*, 2000, **A287**, 178–182.

86. Z. Zhao, V. Buscaglia, P. Bowen and M. Nygren: *Key Eng. Mater.*, 2004, **264–268**, 2297– 2300.

87. S. W. Wang, L. D. Chen and T. Hirai: *J. Mater. Res.*, 2000, **15**, 982–987.

88. L. Gao, J. S. Hong, H. Miyamoto and S. D. D. L. Torre: *J. Eur. Ceram. Soc.*, 2000, **20**, 2149–2152.

89. S.-T. Oh, K.-I. Tajima, M. Ando and T. Ohji: *J. Am. Ceram. Soc.*, 2000, **83**, 1314–1316.

90. Z. Shen, M. Johnsson, Z. Zhao and M. Nygren: *J. Am. Ceram. Soc.*, 2002, **85**, 1921–1927.

91. R. Chaim, Z. Shen and M. Nygren: *J. Mater. Res.*, 2004, **19**, 2527–2531.

92. R. Chaim and M. Margulis: *Mater. Sci. Eng. A*, 2005, **A407**, 180– 187.

93. L. Gao, Q. Li, W. Luan, H. Kawaoka, T. Sekino and K. Niihara: *J. Am. Ceram. Soc.*, 2002, **85**, 1016–1018.

94. J. Wang and L. Gao: *J. Am. Ceram. Soc.*, 2005, **88**, 1637–1639.

95. M. Nygren and Z. Shen: *Solid State Sci.*, 2003, **5**, 125–131.

96. U. Anselmi-Tamburini, J. E. Garay, Z. A. Munir, A. Tacca, F. Maglia and G. Spinolo: *J. Mater. Res.*, 2004, **19**, 3255–3262.

97. U. Anselmi-Tamburini, J. E. Garay, Z. A. Munir, A. Tacca, F. Maglia, G. Chiodelli and G. Spinolo: *J. Mater. Res.*, 2004, **19**, 3263–3269.

98. U. Anselmi-Tamburini, J. E. Garay and Z. A. Munir: *Scripta Mater.*, 2006, **54**, 823–828.

99. M. Nygren and Z. Shen: *Key Eng. Mater.*, 2004, **264–268**, 719–724.

100. S. R. Casolco, J. Xu and J. E. Garay: *Scripta Mater.*, 2008, **58**, 516–519.

101. B. Li, X. Wang, M. Cai, L. Hao and L. Li: *Mater. Chem. Phys.*, 2003, **82**, 173–180.

102. B. Li, X. Wang, L. Li, H. Zhou, X. Liu, X. Han, Y. Zhang, X. Qi and X. Deng: *Mater. Chem. Phys.*, 2004, **83**, 23–28.

103. X. Deng, X. Wang, H. Wen, Z. Kang, Z. Gui and L. Li: *J. Am. Ceram. Soc.*, 2006, **89**, 1059–1064.

104. Z. Zhao, V. Buscaglia, M. Viviani, M. T. Buscaglia, L. Mitoseriu, A. Testino, M. Nygren, M. Johnsson and P. Nanni: *Phys. Rev. B.*, 2004, **70B**, 024107.

105. L. Zhou, Z. Zhao, A. Zimmermann, F. Aldinger and M. Nygren: *J. Am. Ceram. Soc.*, 2004, **87**, 606–611.

106. M. Yoshimura, T. Ohji, M. Sando and K. Niihara: *J. Mater. Sci. Lett.*, 1988, **17**, 1389– 1391.

107. M. Yoshimura, T. Ohji, M. Sando, Y.-H. Choa, T. Sekino and K. Niihara: *Mater. Lett.*, 1999, **38**, 18–21.

108. G.-D. Zhan, J. Kuntz, J. Wan, J. Garay and A. K. Mukherjee: *Scripta Mater.*, 2002, **47**, 737–741.

109. R. Kumar, K. H. Prakash, P. Cheang and K. A. Khor: *Acta Mater.*, 2005, **53**, 2327–2335.

110. C. Elissalde, M. Maglione and C. Estournes: *J. Am. Ceram. Soc.*, 2007, **90**, 973–976.

111. M. Sakai and H. Muto: *Scripta Mater.*, 1998, **6**, 909– 915.

112. H. Muto, Y. Takahashi, T. Futami and M. Sakai: *J. Eur. Ceram. Soc.*, 2002, **22**, 2437– 2442.

113. R. Chaim, R. Ramamoorthy, A. Goldstein, I. Eldror and A. Gurman: *J. Eur. Ceram. Soc.*, 2003, **23**, 647–657.

114. R. Chaim, R. Marder-Jaeckel and J. Z. Shen: *Mater. Sci. Eng.*, 2006, **429**, 74–78.

115. R. Chaim: *J. Mater. Sci.*, 2006, **41**, 7862–7871.